Bonding and Adhesion at the SiC/Fe Interface[†]

Donald F. Johnson[‡] and Emily A. Carter*[,§]

Department of Chemistry, Princeton University, Princeton, New Jersey 08544, and Department of Mechanical and Aerospace Engineering and Program in Applied and Computational Mathematics, Princeton University, Princeton, New Jersey 08544-5263

Received: December 14, 2008; Revised Manuscript Received: February 25, 2009

Ceramics such as SiC have the potential to act as protective coatings, primarily due to their high melting points and wear resistance. We use periodic density functional theory (DFT) within the generalized gradient approximation (GGA) to calculate the adhesion strength between SiC and Fe, for Si- and C-terminations of SiC(100) and two surfaces of Fe: (100) and (110). We predict a maximum ideal work of adhesion of 6.51 J/m^2 at the SiC(100)/Fe(110) interface for C−Fe interfacial bonding, which is stronger than the traditional chrome coating's adherence to Fe. We characterize the interfacial bonding via local densities of states and electron density difference analysis and find strong covalent bonding and some evidence of metallic bonding between Si (C) and Fe. Our results suggest that SiC might prove useful as a thin adhesion layer in a multilayer protective coating for steel.

Introduction

Under the high temperature and pressure conditions present in many industrial applications, coatings must be used to protect steel from thermomechanical failure. Key features of a successful protective coating are wear resistance (e.g., high hardness), high-temperature robustness (e.g., high melting point), corrosion resistance (e.g., formation of a protective oxide scale), and strong adhesion to the substrate being protected. Since chrome coatings satisfy many of these requirements, they are frequently used to protect steel but they fail when inherent microcracks allow deleterious gases to penetrate and erode the Cr/Fe interface.[1,2] Consequently, a new protective coating system has long been desired.[3] Alloying has not proven successful in protecting steel in high-temperature environments. For instance, stainless steel (Cr-doped) offers protection against corrosion, but its melting point is too low. Recently, Jiang and Carter[4] used first principles quantum mechanics calculations to explore whether metal alloys could provide protection against carburization and hydrogen incorporation into steel. They focused on iron alloys that could form stable oxide scales. In particular, they examined FeAl and Fe_3Si surface chemistry but concluded it is difficult to simultaneously prevent H and C incorporation into bulk Fe. As a result, we turned our focus to exploring alternative protective coatings based on ceramic materials rather than metal alloys.

Ceramics have been used in metal matrix composite materials with some success, mainly by employing hard particulates (Zr_2O_3, Y_2O_3, Al_2O_3, TiN, Cr_3C_2, TiC,[5] WC,[6] SiC[7]) to increase wear resistance. In addition to acting as reinforcing agents, ceramics such as yttria-stabilized ZrO_2 (YSZ) are used as protective coatings on Ni-based superalloys in thermal barrier applications. However, YSZ is permeable to oxygen and can only be used when the underlying layers are not adversely affected by significant levels of O_2. Typically an aluminum-containing alloy (e.g., NiAl) is deposited prior to YSZ deposition so that a slow-growing alumina scale develops to protect the underlying metal substrate.[8] Ceramic thin film coatings are widely used to protect other metals (e.g., WC on Co).[9] Recent studies show amorphous silicoaluminum carbonitride (SiAlCN) ceramics exhibit excellent oxidation resistance and are durable under high-temperature conditions.[10]

SiC satisfies many of the requirements of a successful coating candidate. It is a strong, lightweight ceramic with an extremely high melting point (2970 °C) and high hardness.[11] SiC is resistant to corrosion, slowly oxidizing to form an outer silica layer, which makes it a possible candidate for protecting steel. However, silica corrodes in the presence of water vapor[12−15] and many recent efforts in environmental barrier coating (EBC) development have been focused on protecting Si-based ceramics from water vapor via sol−gel processing[16] or EBC methods.[17] SiC also has excellent thermal shock resistance due to its low coefficient of thermal expansion (CTE) and high thermal conductivity. These latter characteristics are not ideal since a low thermal conductivity and higher CTE close to that of steel would be preferred for high-temperature applications. The thermal expansion mismatch should be less of a problem if SiC is used merely as a thin intermediate layer (∼few micrometers) and especially if SiC adheres strongly to the steel substrate. For example, YSZ adheres well to SiC under thermal cycling despite a large difference in the CTE.[18] Since YSZ has very low thermal conductivity, deposition of YSZ on top of SiC may provide thermal protection for high-temperature applications. Thus, we may envision an alternative coating for steel that involves YSZ deposited on SiC that is first deposited on steel. As YSZ is permeable to oxygen, the SiC is expected to develop an oxide scale; earlier quantum mechanics calculations have shown that SiO_2 adheres strongly to zirconia,[19] and the SiO_2 scale is known to bind strongly to SiC.[20] Thus, such an oxide scale would not be expected to destabilize a YSZ/SiC coating on steel.

As mentioned above, one crucial requirement for a resilient EBC is strong adhesion of the coating to the substrate, which remains to be established for SiC on steel. Hence, the purpose

[†]Part of the "George C. Schatz Festschrift".

* Author to whom correspondence may be sent. E-mail: eac@princeton.edu.
[‡] Department of Chemistry.
[§] Department of Mechanical and Aerospace Engineering and Program in Applied and Computational Mathematics.

10.1021/jp8110259 CCC: $40.75
Published on Web 03/13/2009

of this work is to characterize the interaction and quantify the adhesion of SiC on Fe (as a model for steel), as well as to compare the latter to the adhesion of the existing chrome coating. First principles quantum mechanics methods, such as density functional theory (DFT), have been used extensively to characterize such interfacial adhesion but not yet for the SiC/Fe interface. Below we present predictions of the adhesion energy of SiC to Fe and describe the nature of the bonding that occurs at the interface, in order to further assess the viability of SiC as a robust protective coating for steel. While SiC has certain material advantages over Cr, comparing the strength of the SiC/Fe interface to the current Cr/Fe interface is critical. The latter was predicted (using the same level of theory we employ below) to have an ideal adhesion energy of 5.02 J/m^2, due to negligible coating−substrate lattice mismatch and strong magnetic coupling at the interface.[21]

Many metal−ceramic interfaces have been investigated via DFT, but relatively few where Fe is the substrate. DFT calculations predicted good adhesion at the TiC/Fe using both ultrasoft pseudopotentials (USPP)[22] and the full-potential linearized augmented plane wave method.[23] USPP DFT calculations also found good adhesion at the ZrC/Fe[24] interface, due to a mixture of metallic and covalent bonding, while projector augmented wave (PAW)-DFT calculations found even stronger adhesion for $MoSi_2$/Fe,[25] due to formation of strong, covalent Fe−Si bonds. Other DFT studies involving carbide-metal interfaces have investigated the strong WC/Co[26] and WC/Al[27] interfaces and the slightly weaker TiC/Co[28,29] and TiC/Al interfaces.[30]

DFT calculations on SiC itself have investigated the band structures of various hexagonal polytypes[31] and the structure of SiC (110),[32,33] (111),[34] and (100)[35−37] surfaces. Auger electron spectroscopy[38,39] and low-energy electron diffraction[40] experiments on β-SiC support the conclusion that the (100) surface is Si-terminated and dimerized. Weak dimerization was predicted by DFT calculations[37] for bulk-terminated SiC(100), with the dimer length decreasing when the surface is hydrogenated.[41] Taking these results into account, we chose to examine the SiC(100)/Fe(100) and SiC(100)/Fe(110) interfaces for zinc-blende SiC and bcc Fe, as representative interfaces that could be present in a SiC coating on steel substrates. The zinc-blende SiC (100) and body-centered-cubic (bcc) Fe (100) and (110) surfaces are the lowest-energy surfaces in these materials, which thus are the most likely to form stable interfaces. Since the SiC layer next to the Fe substrate in principle could be either C- or Si-terminated, we considered both C−Fe and Si−Fe interfacial bonding at each interface. We also examined the effect of terminating the ceramic coating's free surface with Si dimers (as opposed to simple bulk termination).

Calculational Details

We used the Vienna *ab initio* Simulation Package (VASP)[42,43] to carry out Kohn−Sham (KS) DFT calculations. Calculations for Fe surfaces, SiC surfaces, and SiC/Fe interfaces were carried out spin-polarized to properly treat ferromagnetic Fe and the dangling bonds on the SiC surface, while bulk SiC calculations were performed spin-restricted since there are no dangling bonds or magnetism present in the latter structure. The all-electron (frozen core) PAW method was used to describe the ion−electron interactions[44,45] ("ion" refers to the core electrons and nucleus) and the generalized gradient approximation (GGA) of Perdew, Burke, and Ernzerhof (PBE)[46] was used for the exchange-correlation functional. Standard VASP PAW-GGA-PBE potential files for Fe, Si, C, and H were used in which eight, four, four, and one electrons on each atom, respectively, are variationally optimized. The PAW method was chosen over pseudopotential techniques because the former produces the correct ordering of Fe magnetic states, while standard USPPs fail to do so for some phases of Fe.[47,48] Likewise, the GGA was used instead of the LDA, since the latter predicts the wrong ground state for Fe (hcp instead of bcc).[47,49]

The kinetic energy cutoff for the plane-wave basis set was increased until the total energy of an unrelaxed SiC/Fe interface was converged to within 1 meV/atom, leading to a cutoff of 400 eV for the pseudowavefunctions in all calculations. The cutoff for the augmentation charge was 644 eV (511 eV) for SiC and SiC/Fe (pure Fe) calculations. The k-point sampling was increased until the total energy was converged to within 5 meV/atom. A k-mesh of 15 × 15 × 15 was used for bulk calculations on the primitive cubic cells of Fe and SiC, corresponding to k-point spacings of less than 0.05 (in units of 2π/Å). The converged k-mesh used in the interface calculations resulted in k-point spacings of less than 0.32. The Methfessel−Paxton method was used for Fermi-surface smearing and Brillouin zone integration.[50] The smearing width was 0.1 eV, which ensures an error in total energy < 1 meV/atom, when extrapolated to 0 K.

With these converged parameters, a Murnaghan equation of state fit yields a zinc-blende SiC lattice constant (a) and bulk modulus (B) of 4.37 Å and 210 GPa, respectively. These compare well to previous measurements (a_0 = 4.36 Å,[51] B = 224 GPa[52]) and DFT-GGA calculations[53] (a_0 = 4.34 Å, B = 222 GPa). The equilibrium lattice constant and bulk modulus of bcc Fe were calculated to be 2.834 Å and 174 GPa, respectively, which are also in very good agreement with previous measurements (a_0 = 2.86 Å, B = 168 GPa)[54] and DFT-GGA calculations (a_0 = 2.83 Å, B = 174 GPa).[47]

To construct an interface that is both computationally feasible and experimentally relevant, one must find a small periodically repeating cell which minimizes lattice mismatch between the two materials and is comprised of low-energy surfaces, since these are the ones most likely to form. We calculate the lattice mismatch for a given interface as $1 - [2\Omega/(A_1 + A_2)]$, where A_1, A_2, and Ω are the lateral areas of the substrate periodic cell, the coating periodic cell, and the overlapping area of the two cells, respectively,[55] where the substrate and coating periodic cell areas are taken from the predicted equilibrium structures at 0 K. The smallest mismatch between zinc-blende SiC and bcc Fe is obtained by matching the SiC(100) surface (lowest surface energy) to the Fe(100) surface, which results in a lattice mismatch of only 2.8%. The SiC(100)/Fe(110) interface was also examined (2.9% mismatch), since the (110) surface is the lowest energy surface for bcc Fe. In all calculations, the interface and isolated surface slabs were kept at the bulk Fe substrate lattice parameters in order to mimic a thin coating that adheres epitaxially to a semi-infinite crystalline substrate. Consequently, matching the SiC(100)/Fe(100) interface produces a slight tensile strain in the SiC layer, while the SiC(100)/Fe(110) interface is slightly sheared as well as under slight tensile strain. The strain is kept as small as possible by considering only interface structures with minimum lattice mismatch.

The ideal work of adhesion (W_{ad}) was estimated from the energies of the coating/substrate system and the separated slabs. It is defined as $W_{ad} = (E_1 + E_2 - E_{12})/A$, where E_{12} is the energy of the interface, E_1 is the energy of the coating, E_2 is the energy of the substrate, and A is the area of the interface. "Ideal" refers to the fact that plasticity is not accounted for (and cannot be, on the length scale of these calculations). Despite the fact that

plasticity is neglected, the trends in W_{ad} are expected to be useful predictors of interface stability.

The interface calculations were performed using a 3D periodic supercell consisting of a substrate slab, a ceramic slab, and a vacuum layer. Five layers of Fe were used in all cases, for both the (100) and (110) interfaces. The SiC slab consists of alternating (100) layers of Si or C atoms, keeping the surface facing vacuum always Si-terminated, since this termination is most stable. Therefore, Si−Fe (C−Fe) interface bonding was simulated using an odd (even) number of SiC layers in the SiC coating. By this construction, the SiC slab is nonstoichiometric for an odd number of layers. The SiC coating was translated laterally with respect to the Fe substrate to determine the lowest-energy initial guess structure while maximizing overlap of interface atoms with hollow sites on the Fe substrate surface, which were determined to be the preferred interaction sites for atoms in the coating's first layer.

On the as-cleaved SiC(100) surface, each surface atom has two dangling bonds, prior to any reconstruction that may occur. Since there is evidence of Si dimers on the (100) surface,[38−40] we tested bulk termination (Si layer) and dimer termination (with H atoms quenching dangling bonds). This was found to have little (< 5%) effect on the calculated W_{ad} of the (100)/(100) interface, and hence, only bulk-terminated SiC was used to model the (100)/(110) interface. In order to eliminate interaction of the free surface with the interface, the SiC slab thickness was increased until the calculated adhesion energy no longer changed.

When C−Fe interface bonding is modeled, the separated SiC slab is C-terminated on one side. The SiC(100) surface naturally occurs only with Si-termination; no C-terminated surface has been observed upon (100) cleavage of bulk SiC. However, low-energy electron diffraction experiments[56] suggest that carbon dimers can form on Si−Si bridge sites, but only in the presence of C_2H_4 cracking at high temperature, a condition not relevant to our situation. We therefore do not allow C−C dimerization at the interface side of the separated ceramic slab, in order to calculate the direct energy cost of breaking C−Fe cross-interface bonds, without inconsistent, finite size artifacts of the model entering the calculation. While C−C dimers at Si bridge sites are not relevant to our simulation, DFT does predict a different reconstruction, where neighboring C atoms move toward each other to quench dangling bonds. Unfortunately, dimerization of C-terminated surfaces of the thin SiC coatings considered here, which are under tensile and sometimes shear strain, results in large distortions and a breakdown of the zinc-blende structure, which is clearly not representative of a micrometers-thick coating expected to retain its bulk crystal structure. For isolated, unstrained, thicker (≥12 layers) SiC slabs, we find that a SiC(100) $c(2 \times 2)$ reconstruction with C dimers can form without destruction of the zinc-blende structure, resulting in a net energy gain of up to 1.99 eV per surface C atom (or 3.17 J/m^2), similar to previous DFT-LDA predictions.[57] To arrive at an interfacial adhesion that converges with slab thickness, we use the local minimum in energy of the fully atomically-relaxed, unreconstructed C-terminated surface as the final state of the SiC slab. Then, a lower bound to the adhesion energy may be obtained by subtracting the reconstruction (dimerization) energy of 3.17 J/m^2 listed above from the adhesion energy derived from the unreconstructed SiC(100) surface.

In order to obtain minimum energy structures, the atomic positions were relaxed to within a force tolerance of 0.03 eV/Å. The bottom two layers of the substrate Fe slab were held fixed to bulk positions in order to mimic a semi-infinite bulk crystal, resulting in residual forces on these fixed atoms of ≥0.20 eV/Å. The total energy change upon relaxing the third layer is small, about 5 meV; therefore, three structurally relaxed layers should be a sufficient substrate model. All atomic positions in the coating are relaxed, within the constraint that the SiC lattice vectors parallel to the interface remained equal to those of the substrate. By keeping the separated SiC slab constrained to the bulk Fe lattice vectors parallel to the interface, elastic strain energies approximately cancel between the interface and the free SiC slab.[58−60] This constraint makes the W_{ad} calculated here an upper bound to the ideal work of adhesion. It is not an upper bound to the true adhesion energy since, as mentioned above, plastic dissipation (e.g., dislocation nucleation and motion) cannot be accounted for at this length scale. Trends in the ideal adhesion energy nonetheless are useful for comparing intrinsic bonding and strengths of related interfaces.

We also calculated the change in electron density upon the formation of the interface, a useful tool to visualize where bonds are forming. A simple difference is taken: $\Delta\rho = \rho_{FeSiC} - \rho_{Fe} - \rho_{SiC}$, where ρ_{FeSiC} is the electron density of the structurally relaxed interface and ρ_{Fe} and ρ_{SiC} are the electron densities of isolated slabs constructed with atomic positions identical to those in the interface slab. This ensures that the only changes in electron density we record are those due to the fact that the interface has formed (and none due to movement of nuclei). As a post-calculation analysis, we project the KS orbitals (within atom-centered spheres) onto localized atomic orbitals. Standard Wigner−Seitz radii of 1.302, 1.312, and 0.863 Å are used for the projection spheres of Fe, Si, and C to obtain site-projected local densities of states (LDOS).

Results and Discussion

In what follows, $SiC(100)_{Si}$ refers to the ceramic slab terminated with a Si layer at the interface leading to Si−Fe interfacial bonding. Similarly, $SiC(100)_C$ refers to the C-terminated slab and C−Fe interfacial bonding. In all cases, the free surface of SiC (not at the interface) is bulk-terminated with a Si layer, i.e., no reconstruction of the outer surface is allowed, again in order to mimic a thicker coating. First, we report the converged values of the ideal work of adhesion W_{ad} for the different interfaces. We then discuss the structure and bonding at the interfaces. Finally we compare the $SiC(100)_{Si}$/Fe interfacial bonding to the $Si(100)_C$/Fe bonding in order to explain trends in the ideal W_{ad}.

The ideal W_{ad} was converged with respect to the number of ceramic layers for the four distinct interfaces mentioned previously. The $SiC(100)_{Si}$/Fe(100) interface converged to a W_{ad} value of 3.20 J/m^2 at nine layers of SiC, whereas the $SiC(100)_C$/Fe(100) interface has a much higher converged W_{ad} of 5.74 J/m^2 at eight layers of SiC. At the SiC(100)/Fe(110) interface, both terminations exhibit stronger adhesion than the (100)/(100) interface: 3.63 J/m^2 and 6.51 J/m^2, respectively, for $SiC(100)_{Si}$/Fe(110), again converged at nine layers of SiC, and for $SiC(100)_C$/Fe(110), again converged at eight layers of SiC. However, if C−C dimerization of the separated, C-terminated SiC slab were to occur, the adhesion energy would decrease by ∼3.17 J/m^2 (via the final state of the SiC slab relaxing to a lower total energy). Then the final-state-adjusted values for the W_{ad} of $SiC(100)_C$/Fe(100) and $SiC(100)_C$/Fe(110) would be 2.57 and 3.34 J/m^2, respectively. Thus, we find that the intrinsic strengths of interfaces with C closest to the Fe substrate are much higher than when Si is closest to the Fe substrate. However, if the SiC coating delaminates in such a way as to allow for surface reconstruction, the adhesion energy would

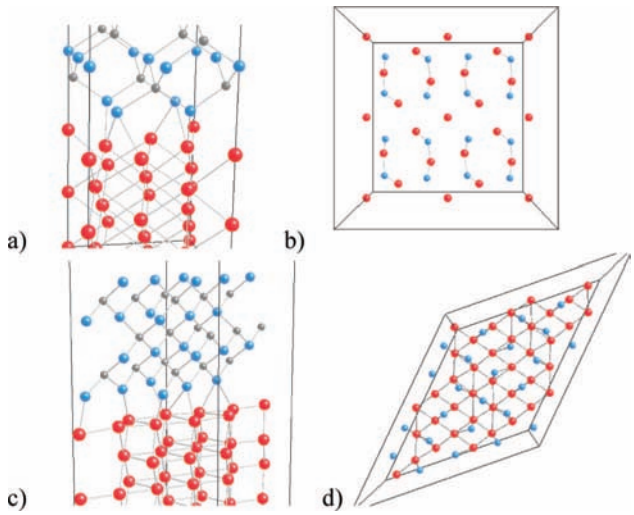

Figure 1. Relaxed interface geometry for $SiC(100)_{Si}$/Fe(100) (a,b) and $SiC(100)_{Si}$/Fe(110) (c,d) interfaces. Bonds with length ≤2.6 Å are drawn. Atoms at cell boundaries have their periodic images shown. Top views (b and d) depict only the two interface layers and show four periodic cells. Color online: Fe (red), Si (blue), C (gray).

decrease by the energy released by this process, leaving these interfaces ultimately weaker than those with Si closest to the Fe substrate.

To put these values in context, the intrinsic adhesion of Fe to itself (twice the surface energy, 2γ) is 4.4 J/m^2 and 4.8 J/m^2 for the (100) and (110) surfaces, respectively, and the adhesion of Cr to Fe was already mentioned to be 5.0 J/m^2. Thus, if the C-terminated SiC/Fe interface does not reconstruct upon delamination, the prediction is that such a coating would be more stable than the current Cr/Fe coating. However, if such a reconstruction were to occur upon delamination, then the SiC_{Si}/Fe coating would be more stable than the SiC_C/Fe coating but less stable than the current Cr/Fe coating. The rest of this section is devoted to digging deeper to glean an understanding into the trends in ideal works of adhesion discussed above, by examining the structure and bonding in each coating.

SiC(100)/Fe(100). At the SiC(100)/Fe(100) interface (Figure 1a,b), there are five Fe atoms for every four Si (or C) atoms in each unit cell. In the case of $SiC(100)_{Si}$/Fe(100), Si relaxes slightly toward the four-fold hollow sites on the Fe surface (Figure 1b). The stiff SiC bond angles prevent full relaxation, compared to other coatings such as $MoSi_2$/Fe,[25] where Si was found to penetrate deeper into the Fe layer. As a result, the Si atoms at the SiC/Fe interface each form one strong bond to a single Fe atom. These bond lengths are between 2.24 and 2.29 Å. The "lone" Fe atom at the interface without a short bond to a Si atom actually relaxes away from the Fe layer and toward the Si layer, forming four long "bonds" to the four Si atoms (∼2.88 Å). Averaging the distances perpendicular to the interfacial plane, the lone Fe atom is 1.64 Å from the Si layer, while the other four Fe atoms are 1.91 Å from the Si layer. By taking half the room temperature bond lengths in bcc Fe, diamond Si, and diamond C, one can estimate atomic radii for Fe, Si, and C of 1.243, 1.176, and 0.772 Å, respectively.[54] Thus, we might expect Fe−Si bond lengths roughly equal to the sum of their respective radii, i.e., Fe−Si bond lengths about 2.42 Å, consistent with the 2.43 Å Fe−Si bond lengths in bulk Fe_3Si.[4] Instead, we see that the four Fe−Si short bonds at the interface are significantly shorter than this, suggesting formation of quite strong cross-interface bonds.

When C comprises the first ceramic layer on top of the Fe substrate, even more noticeable structural relaxation occurs (Figure 2a,b). Each C atom at the interface has one short bond to a unique Fe atom (1.86−1.88 Å) and two longer bonds (2.05−2.51 Å). The Fe−C bond lengths are shorter than those expected from summing atomic radii, 2.02 Å, and most nearest-neighbor Fe−C bonds in cementite (Fe_3C), 1.88−2.18 Å.[61] These Fe−C bonds at the interface are not traditional covalent bonds, since the C atoms at the surface of the SiC coating already each form two covalent bonds to Si atoms in the next SiC layer, leaving only two C valence electrons available to interact with the Fe atoms. Since these C atoms each form three bonds to Fe, some delocalization/sharing of electrons must be occurring, which can be characterized then as a mixture of metallic and covalent bonds. The "lone" Fe atom in each unit

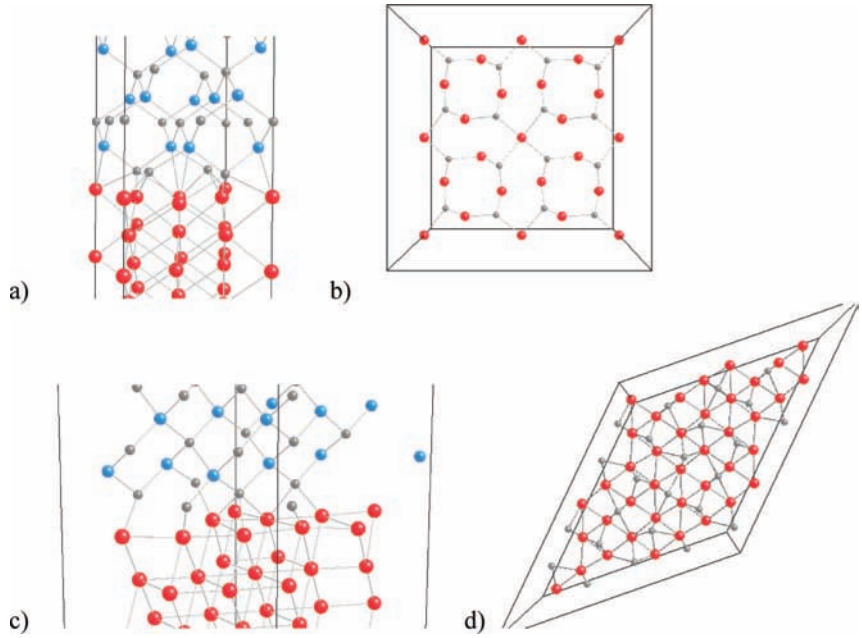

Figure 2. Relaxed interface geometry for $SiC(100)_C$/Fe(100) (a,b) and $SiC(100)_C$/Fe(110) (c,d) interfaces. Bonds with length ≤2.6 Å are drawn. Atoms at cell boundaries have their periodic images shown. Top views (b and d) depict only the two interface layers and show four periodic cells. Color online: Fe (red), Si (blue), C (gray).

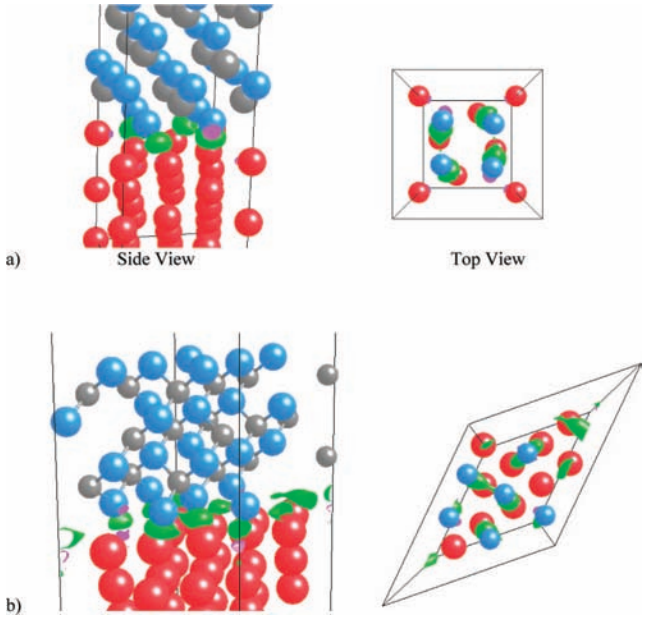

Figure 3. Si−Fe cross-interface bonding at the (a) $SiC(100)_{Si}$/Fe(100) interface and (b) $SiC(100)_{Si}$/Fe(110) interface. Green (pink) isosurfaces represent increased (decreased) electron density upon formation of the interface. The formation of Si−Fe interface bonds is shown by increased electron density within the green isosurface (+0.05 e/Å^3). Areas of decreasing electron density are shown by the pink isosurface (−0.05 e/Å^3).

cell has long bond lengths to all four C atoms (2.32−2.51 Å) and to two Si atoms (2.60 Å) in the next layer, suggesting that it forms weak interactions with both the C surface atoms and the Si subsurface atoms. Again, averaging the interface−normal distances shows the lone Fe atom sits 0.27 Å closer to the C layer than the other four Fe atoms. Si−C bond lengths inside the SiC coating are 1.90−1.93 Å for all arrangements, which is similar to the equilibrium Si−C bond length we find for in bulk zinc-blende SiC (1.89 Å).

Visualization of the electron density differences that result upon formation of the $SiC(100)_{Si}$/Fe(100) interface (Figure 3a) reveals the location of the four Si−Fe bonds. The only significant density change is a large electron density accumulation that occurs along these bonds, which attests to their localized, covalent character. A representative Fe−Si interface bond then was selected and the atom-projected LDOS for these two atoms is shown in Figure 4a. The close overlap between the Fe 3d and 4s states and the Si 3sp states below (covalent bonding states) and above (covalent antibonding states) the Fermi level is more evidence of strong covalent bonding at the interface. A significant density of states at the Fermi level is also present, indicating metallic character is also present in the interfacial bonding.

At the $SiC(100)_C$/Fe(100) interface, the electron density differences are strikingly different than the case with Si termination. Here the C atoms form multiple, partially delocalized bonds to the Fe atoms (Figure 5a), consistent with our analysis above that each C atom interaction with three Fe atoms requires some delocalized bonding to occur. The projected LDOS of the C−Fe bond (Figure 6a) again shows strong overlap between the C 2p and the Fe 3d LDOS above and below the Fermi level. This indicates covalent bonding is largely responsible for the strong interface adhesion, although these LDOS also have significant population at the Fermi level, suggesting delocalized metallic bonding also contributes.

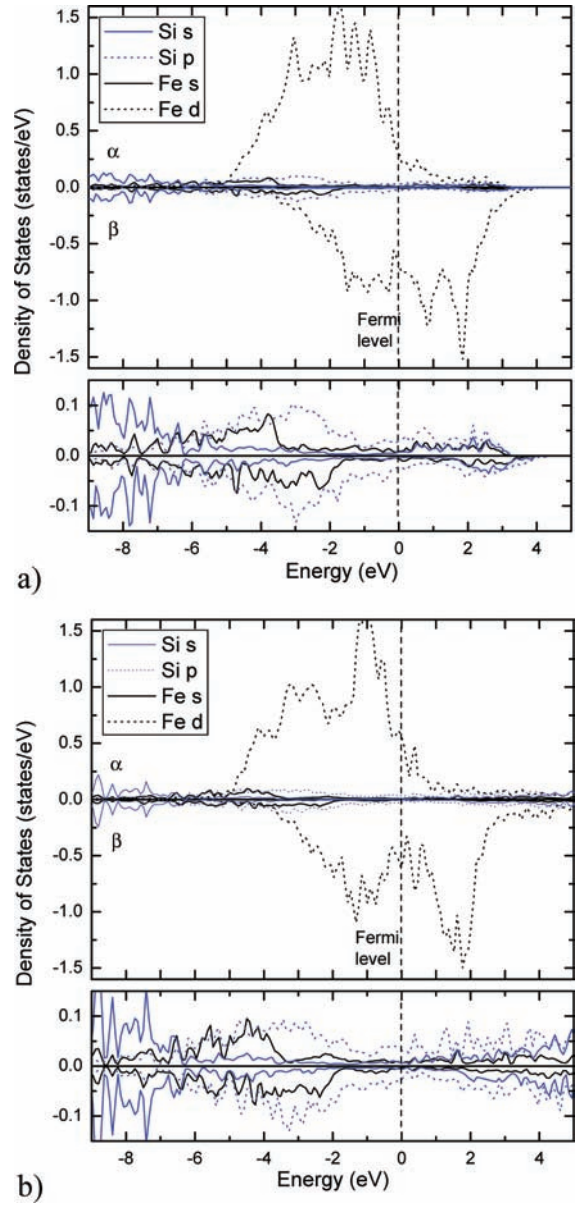

Figure 4. LDOS at the (a) $SiC(100)_{Si}$/Fe(100) interface and the (b) $SiC(100)_{Si}$/Fe(110) interface for a representative Si−Fe bond. Positive (negative) LDOS refers to the majority α (minority β) spin states. The same convention is used in all LDOS plots. The vertical axis is enlarged at the bottom of each figure to show Si sp and Fe s states more clearly.

SiC(100)/Fe(110). For the SiC(100)/Fe(110) interface, we again consider the two cases where either Si or C atoms occupy the first ceramic layer. There are 10 Fe atoms and six Si (or C) atoms at the interface (Figure 1c,d) of each unit cell.

At the $SiC(100)_{Si}$/Fe(110) interface, the cross-interface Si−Fe bonds range from 2.26 to 2.67 Å and the average Si layer−Fe layer distance is 2.00 Å, exactly the same as the (110) layer spacing in bulk Fe but much larger than the spacing between C layers and Si layers in SiC (1.10 Å). Four Si atoms have one short (2.26 Å) and one longer bond (2.48 or 2.67 Å) to Fe, while the other two Si atoms each make two bonds of equal length (~2.36 Å) to Fe. Most bonds are shorter than those in Fe_3Si (2.43 Å) and shorter than those expected from sums of atomic radii (2.42 Å), suggesting formation of strong covalent bonds. Further evidence for each Si atom forming roughly one covalent bond to each of two Fe atoms is given by the

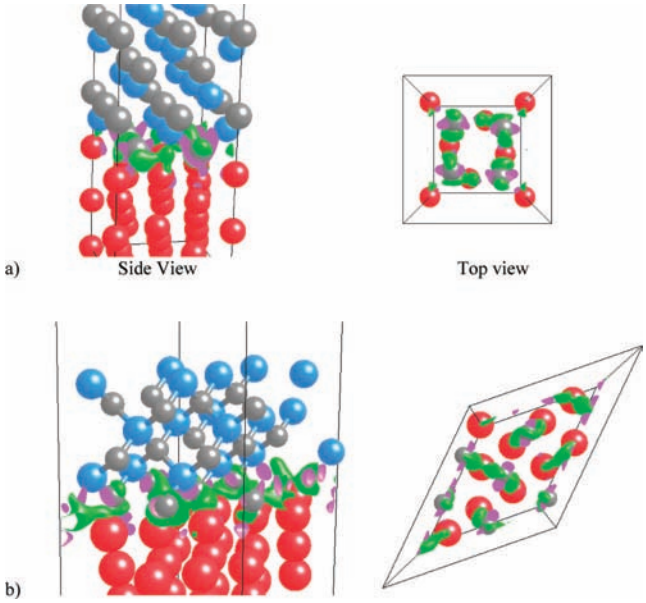

Figure 5. C−Fe cross-interface bonding at the (a) $SiC(100)_C$/Fe(100) interface and (b) $SiC(100)_C$/Fe(110) interface. Green (pink) isosurfaces represent increased (decreased) electron density upon formation of the interface. Formation of C−Fe interface bonds are shown by the green isosurface (+0.05 e/Å^3). The electron density decreases in areas designated by pink isosurface (−0.05 e/Å^3).

accumulated electron density that is localized along the Si−Fe bond axes (Figure 3b), indicating covalent bonding at the interface.

We again select a representative Fe−Si interface bond to calculate the atom-projected LDOS for the corresponding Fe and Si atoms, displayed in Figure 4b. The atom-projected LDOS here is very similar to the Si−Fe LDOS profile at the (100)/(100) interface (Figure 4a). There is again strong overlap of the Fe sd states and the Si p states above and below the Fermi level, indicating covalent bonding, as well as significant density of states at the Fermi level, for both Fe and Si, indicating metallic bonding also contributes.

When C is present at the interface (Figure 2c,d), relaxation toward hollow sites is similar to SiC_{Si}/Fe relaxation, but the C−Fe bond lengths (from 1.84 Å to 2.18 Å) are smaller than Si−Fe bond lengths since C is smaller than Si. In fact, 10 C−Fe bonds in the unit cell are shorter than the C−Fe bond length expected from metal radii, 2.02 Å. The $SiC(100)_C$/Fe(110) interface exhibits a large buildup of electron density along the Fe−C bonds (Figure 5b), even more so than for the Fe−Si bonds (Figure 3b). The smaller C atoms penetrate deeper into the Fe interface layer and also allow the second-layer Si atoms to interact with the Fe interface atoms. The C 2p and Fe 3d states overlap well below −5 eV and above 1 eV (Figure 6b). Once again, the DOS has significant population at the Fermi level. This suggests again that a mixture of metallic and covalent bonding is taking place at the interface.

We are now in a position to rationalize the trends in predicted adhesion energies. A significant difference exists in the structures of the SiC_{Si}/Fe and SiC_C/Fe interfaces, most notably the higher coordination of the atoms at the latter interface. Due to the smaller size of C compared to that of Si, the C−Fe bonds are shorter and the C layer sits closer to the Fe layer. The dense packing of the SiC_C/Fe interface layers puts Si atoms in close proximity to Fe atoms, resulting in favorable Si−Fe interactions as well. The bonding of Fe atoms to interface C atoms and interactions with second-layer Si atoms produces the larger calculated W_{ad} for the SiC_C/Fe interfaces.

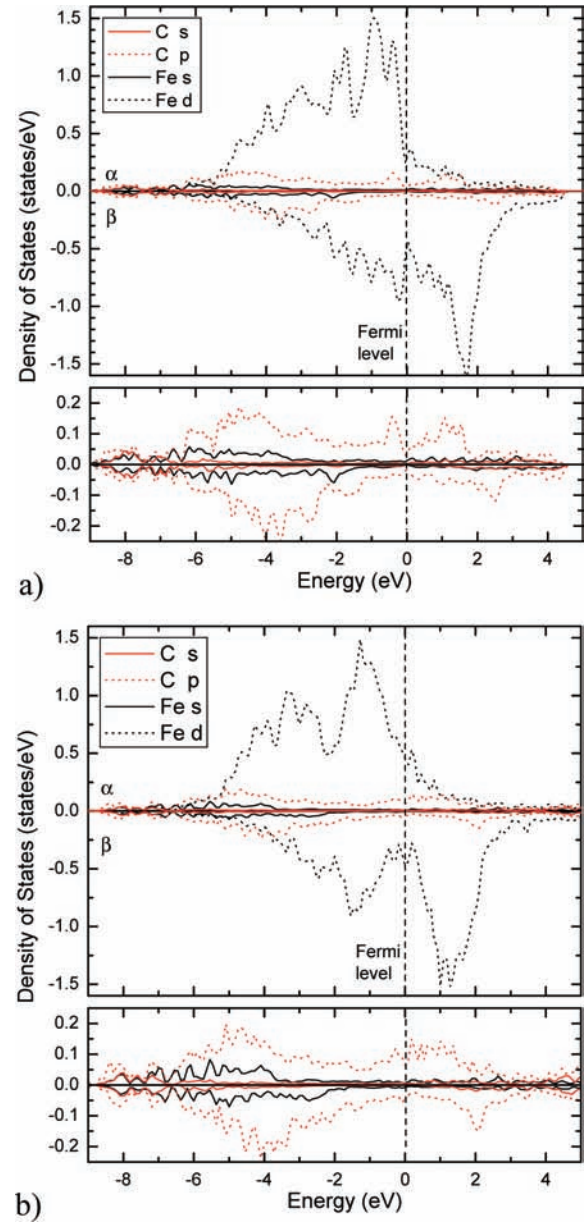

Figure 6. Projected LDOS for C (red) and Fe (black) at the (a) $SiC(100)_C$/Fe(100) interface and the (b) $SiC(100)_C$/Fe(110) interface for a representative C−Fe bond. The vertical axis is enlarged at the bottom of each figure to show C sp and Fe s states more clearly.

The intrinsic W_{ad}, 2γ, for Fe (4.8 J/m^2) and unreconstructed SiC (9.92 J/m^2) are both much higher than the Si−Fe bonded interface (3.20 and 3.63 J/m^2), but the C−Fe bonded interface is intermediate between the two (5.74 and 6.51 J/m^2). Our predicted interface adhesion trends (C−Fe bonds intrinsically stronger than Si−Fe bonds) are consistent with related experimental bulk cohesive energies: Fe_3C has a cohesive energy of E_{coh} = 5.05 eV/atom,[62] which is larger than that of Fe_3Si (E_{coh} = 4.67 eV/atom).[63] Thus, the intrinsically stronger Fe−C bonds should result in a stronger interface. However, if a reconstruction of the SiC surface occurs upon interface cleavage, this would substantially weaken this interface relative to the interface formed by a SiC coating with Si at the interface. Consequently, it cannot be concluded with certainty that SiC adheres more strongly to Fe than Cr, but it is likely strong enough to serve as a protective coating.

Conclusions

First principles PAW-DFT-GGA calculations were performed for the SiC (001)/Fe (001) and SiC(001)/Fe(110) interfaces. Adhesion of SiC/Fe was found to be stronger on the Fe(110) surface and strongest when C−Fe bonds were present at the interface. The greatest adhesion is predicted at the $SiC(100)_C$/Fe(110) interface with a $W_{ad} = 6.51$ J/m^2. However, this is a prediction of the energy cost to break the C−Fe bonds and not reflective of a reconstructed C-terminated SiC final state. If such a reconstruction occurs upon delamination of the coating, then the SiC coating with Si at the interface would be thermodynamically favored. A mixture of metallic and multiple covalent bonds is responsible for the very strong adhesion at the interface between Fe and SiC. The strong adhesion makes SiC a possible EBC for certain applications such as high pressure vessels. It might be employed as a thin layer in a multilayer EBC system in harsh, high temperature environments. A multilayer coating that includes YSZ and a silica scale on top of a SiC layer may provide the steel substrate with a useful balance of thermal protection and chemical resistance.

Acknowledgment. This work was supported by a grant from the Army Research Office. Computations were performed on IBM NH-2 SMP P3 machines at the ARL MRSC in Maryland and IBM P4 machines at ARSC in Alaska. We are pleased to dedicate this article to George Schatz, whose wide-ranging contributions to theoretical chemistry increasingly include materials phenomena such as described here.

References and Notes

(1) Turley, D. M. *Wear* **1989**, *131*, 135.
(2) Cote, P. J.; Rickard, C. *Wear* **2000**, *241*, 17.
(3) Carter, R. H. *J. Pressure Vessel Technol.-Trans. Asme* **2006**, *128*, 251.
(4) Jiang, D. E.; Carter, E. A. *J. Phys. Chem. B* **2005**, *109*, 20469.
(5) Pagounis, E.; Lindroos, V. K. *Mater. Sci. Eng., A* **1998**, *246*, 221.
(6) Zhang, G. S.; Xing, H. D.; Gao, Y. L. *Wear* **2006**, *260*, 728.
(7) Pelleg, J. *Mater. Sci. Eng., A* **1999**, *269*, 225.
(8) Padture, N. P.; Gell, M.; Jordan, E. H. *Science* **2002**, *296*, 280.
(9) Lovelock, H. L. D. *J. Thermal Spray Technol.* **1998**, *7*, 357.
(10) An, L. N.; Wang, Y. G.; Bharadwaj, L.; Zhang, L. G.; Fan, Y.; Jiang, D. P.; Sohn, Y. H.; Desai, V. H.; Kapat, J.; Chow, L. C. *Adv. Eng. Mater.* **2004**, *6*, 337.
(11) Kim, Y. W.; Park, S. W.; Lee, J. G. *J. Mater. Sci. Lett.* **1995**, *14*, 1201.
(12) Tortorelli, P. F.; More, K. L. *J. Am. Ceram. Soc.* **2003**, *86*, 1249.
(13) Opila, E. J.; Hann, R. E. *J. Am. Ceram. Soc.* **1997**, *80*, 197.
(14) Opila, E. J.; Smialek, J. L.; Robinson, R. C.; Fox, D. S.; Jacobson, N. S. *J. Am. Ceram. Soc.* **1999**, *82*, 1826.
(15) More, K. L.; Tortorelli, P. F.; Walker, L. R.; Miriyala, N.; Price, J. R.; van Roode, M. *J. Am. Ceram. Soc.* **2003**, *86*, 1272.
(16) Kim, H.; Chen, A.; Yang, Q.; Troczynski, T. *Mater. Sci. Eng., A* **2006**, *420*, 150.
(17) Lee, K. N.; Fox, D. S.; Eldridge, J. I.; Zhu, D. M.; Robinson, R. C.; Bansal, N. P.; Miller, R. A. *J. Am. Ceram. Soc.* **2003**, *86*, 1299.
(18) Lee, K. N.; Miller, R. A. *Surf. Coat. Technol.* **1996**, *87*−*88*, 142.
(19) Jarvis, E. A. A.; Carter, E. A. *J. Am. Ceram. Soc.* **2003**, *86*, 373.
(20) Chang, S. Y.; Huang, Y. C. *Microelectron. Eng.* **2007**, *84*, 319.
(21) Johnson, D. F.; Jiang, D. E.; Carter, E. A. *Surf. Sci.* **2007**, *601*, 699.
(22) Arya, A.; Carter, E. A. *J. Chem. Phys.* **2003**, *118*, 8982.
(23) Lee, J. H.; Shishidou, T.; Zhao, Y. J.; Freeman, A. J.; Olson, G. B. *Philos. Mag.* **2005**, *85*, 3683.
(24) Arya, A.; Carter, E. A. *Surf. Sci.* **2004**, *560*, 103.
(25) Jiang, D. E.; Carter, E. A. *Acta Mater.* **2005**, *53*, 4489.
(26) Christensen, M.; Dudiy, S.; Wahnstrom, G. *Phys. Rev. B: Condens. Mater. Phys.* **2002**, *65*, 9.
(27) Siegel, D. J.; Hector, L. G.; Adams, J. B. *Surf. Sci.* **2002**, *498*, 321.
(28) Dudiy, S. V.; Lundqvist, B. I. *Phys. Rev. B.* **2001**, *64*, 045403.
(29) Dudiy, S. V.; Hartford, J.; Lundqvist, B. I. *Phys. Rev. Lett.* **2000**, *85*, 1898.
(30) Liu, L. M.; Wang, S. Q.; Ye, H. Q. *J. Phys.: Condens. Matter* **2004**, *16*, 5781.
(31) Kackell, P.; Wenzien, B.; Bechstedt, F. *Phys. Rev. B: Condens. Mater. Phys.* **1994**, *50*, 10761.
(32) Wenzien, B.; Kackell, P.; Bechstedt, F. *Surf. Sci.* **1994**, *309*, 989.
(33) Sabisch, M.; Kruger, P.; Pollmann, J. *Phys. Rev. B: Condens. Mater. Phys.* **1995**, *51*, 13367.
(34) Wenzien, B.; Kackell, P.; Bechstedt, F. *Surf. Sci.* **1995**, *333*, 1105.
(35) Kackell, P.; Furthmuller, J.; Bechstedt, F. *Appl. Surf. Sci.* **1996**, *104*, 45.
(36) Catellani, A.; Galli, G. *Prog. Surf. Sci.* **2002**, *69*, 101.
(37) Kackell, P.; Bechstedt, F.; Husken, H.; Schroter, B.; Richter, W. *Surf. Sci.* **1997**, *391*, L1183.
(38) Kaplan, R. *Surf. Sci.* **1989**, *215*, 111.
(39) Dayan, M. *J. Vac. Sci. Technol., A* **1986**, *4*, 38.
(40) Powers, J. M.; Wander, A.; Vanhove, M. A.; Somorjai, G. A. *Surf. Sci.* **1992**, *260*, L7.
(41) Peng, X. Y.; Ye, L.; Wang, X. *Surf. Sci.* **2004**, *571*, 21.
(42) Kresse, G.; Furthmuller, J. *Phys. Rev. B: Condens. Mater. Phys.* **1996**, *54*, 11169.
(43) Kresse, G.; Furthmuller, J. *Comput. Mater. Sci.* **1996**, *6*, 15.
(44) Kresse, G.; Joubert, D. *Phys. Rev. B: Condens. Mater. Phys.* **1999**, *59*, 1758.
(45) Blochl, P. E. *Phys. Rev. B: Condens. Mater. Phys.* **1994**, *50*, 17953.
(46) Perdew, J. P.; Burke, K.; Ernzerhof, M. *Phys. Rev. Lett.* **1996**, *77*, 3865.
(47) Jiang, D. E.; Carter, E. A. *Phys. Rev. B: Condens. Mater. Phys.* **2003**, *67*, 214103.
(48) Cocula, V.; Pickard, C. J.; Carter, E. A. *J. Chem. Phys.* **2005**, *123*, 214101.
(49) Moroni, E. G.; Kresse, G.; Hafner, J.; Furthmuller, J. *Phys. Rev. B: Condens. Mater. Phys.* **1997**, *56*, 15629.
(50) Methfessel, M.; Paxton, A. T. *Phys. Rev. B: Condens. Mater. Phys.* **1989**, *40*, 3616.
(51) Madelung, O., Schultz, M., Weiss, H., Eds. *Physics of Group-IV and III-V Compounds*; Springer-Verlag: Berlin, 1982; Vol. 17.
(52) Yean, D. H.; Riter, J. R. *J. Phys. Chem. Solids* **1971**, *32*, 653.
(53) Karch, K.; Pavone, P.; Windl, W.; Strauch, D.; Bechstedt, F. *Int. J. Quantum Chem.* **1995**, *56*, 801.
(54) Kittel, C. *Introduction to Solid State Physics*, 7th ed.; Wiley: New York, 2002.
(55) Christensen, A., Jarvis, E. A. A., Carter, E. A. In *Chemical Dynamics in Extreme Environments*; Dressler, R. A., Ng, C., Eds.; World Scientific: Singapore, 2001; Vol. 11; pp 490.
(56) Powers, J. M.; Wander, A.; Rous, P. J.; Vanhove, M. A.; Somorjai, G. A. *Phys. Rev. B: Condens. Mater. Phys.* **1991**, *44*, 11159.
(57) Kackel, P.; Furthmuller, J.; Bechstedt, F. *Surf. Sci.* **1996**, *352*, 55.
(58) Christensen, A.; Carter, E. A. *Phys. Rev. B: Condens. Mater. Phys.* **2000**, *62*, 16968.
(59) Zhang, W.; Smith, J. R.; Wang, X. G.; Evans, A. G. *Phys. Rev. B: Condens. Mater. Phys.* **2003**, *67*, 12.
(60) Carling, K. M.; Carter, E. A. *Acta Mater.* **2007**, *55*, 2791.
(61) Chiou, W. C.; Carter, E. A. *Surf. Sci.* **2003**, *530*, 87.
(62) Haglund, J.; Guillermet, A. F.; Grimvall, G.; Korling, M. *Phys. Rev. B: Condens. Mater. Phys.* **1993**, *48*, 11685.
(63) Sommer, F. *J. Therm. Anal.* **1988**, *33*, 15.

JP8110259